Design Principles for Trap-Free $CsPbX_3$ Nanocrystals: Enumerating and Eliminating Surface Halide Vacancies with Softer Lewis Bases

David P. Nenon,[†,⊥] Kimo Pressler,[†] Jun Kang,[⊥] Brent A. Koscher,[†,⊥] Jacob H. Olshansky,[†,⊥] Wojciech T. Osowiecki,[†,⊥] Matthew A. Koc,[†,⊥] Lin-Wang Wang,[⊥] and A. Paul Alivisatos*[,†,⊥,§,#]

†Department of Chemistry, #Department of Materials Science and Engineering, University of California, Berkeley, Berkeley, California 94720, United States

⊥Material Sciences Division, Lawrence Berkeley National Laboratory, Berkeley, California 94720, United States

§Kavli Energy NanoScience Institute, Berkeley, California 94720, United States

*Author to whom correspondence should be addressed

ABSTRACT

We introduce a general surface passivation mechanism for cesium lead halide perovskite materials ($CsPbX_3$, X = Cl, Br, I) that is supported by a combined experimental and theoretical study of the nanocrystal surface chemistry. A variety of spectroscopic methods are employed together with *ab initio* calculations to identify surface halide vacancies as the predominant source

of charge trapping. The number of surface traps per nanocrystal is quantified by ^{1}H NMR spectroscopy, and that number is consistent with a simple trapping model in which surface halide vacancies create deleterious under-coordinated lead atoms. These halide vacancies exhibit trapping behavior that differs between $CsPbCl_3$, $CsPbBr_3$, and $CsPbI_3$. *Ab initio* calculations suggest that introduction of anionic X-type ligands can produce trap-free bandgaps by altering the energetics of lead-based defect levels. General rules for selecting effective passivating ligand pairs are introduced by considering established principles of coordination chemistry. Introducing softer, anionic, X-type Lewis bases that target under-coordinated lead atoms results in absolute quantum yields approaching unity and monoexponential luminescence decay kinetics, thereby indicating full trap passivation. This work provides a systematic framework for preparing highly luminescent $CsPbX_3$ nanocrystals with variable compositions and dimensionalities, thereby improving fundamental understanding of these materials and informing future synthetic and post-synthetic efforts towards trap-free $CsPbX_3$ nanocrystals.

INTRODUCTION

Essentially trap-free nanocrystals represent optimal building blocks for optoelectronic technologies, as these materials possess high luminescence efficiencies,[1-3] narrow fluorescence linewidths, excellent photostability, and tunable absorption and emission.[4-9] Inorganic cesium lead halide ($CsPbX_3$, X = Cl, Br, I) perovskite nanocrystals offer an appealing alternative to prototypical metal chalcogenide nanocrystals, as they represent an important class of ionic, defect-tolerant semiconductors with tunable emission in the visible spectrum.[10-17] The defect tolerance of $CsPbX_3$ nanocrystals is a major enabling factor in their bright photoluminescence without a passivating shell.[18-20] However, the quantum yields of these nanocrystals do not yet regularly approach unity. The utility of devices based on $CsPbX_3$ nanocrystals is currently limited by incomplete

understanding of their surface chemistry and the underlying charge trapping pathways that prevent near-unity photoluminescence quantum yield. Addressing these challenges not only has the potential to greatly enhance the utility of this new class of nanocrystals, but also to increase understanding of charge trapping and ligand binding for highly ionic semiconductor surfaces.

Termination of an extended inorganic solid crystal inherently creates under-coordinated atoms, making surface traps a ubiquitous challenge for nanocrystals.[21-30] The pursuit of trap-free nanocrystals is thus intimately intertwined with identification and passivation of surface defects.

Scheme 1. Nanocrystal Ligand Binding Motifs According to the Covalent Bond Classification Method

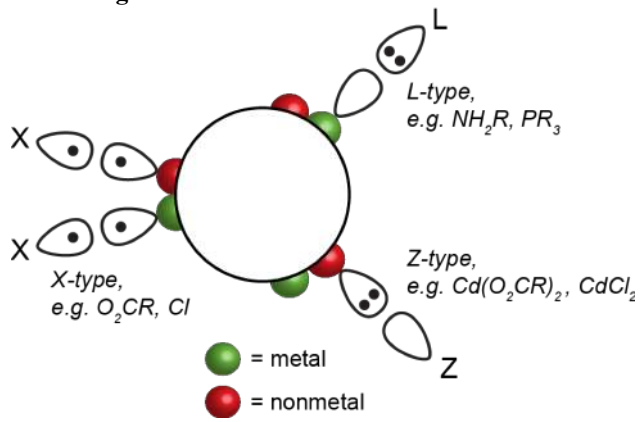

Typically, passivation is achieved by employing an epitaxial shell of a larger bandgap material[1, 31] or through the use of capping ligands.[32-35] Passivating ligands are a particularly promising option, as a larger bandgap shell introduces a tunneling barrier that hinders charge extraction.[36] Ligands can bind to nanocrystal surfaces in a variety of motifs, well described by the Covalent Bond Classification.[37] Scheme 1 depicts L-, X-, and Z-type ligands, which are classified by the number of electrons (2, 1, and 0, respectively) that the neutral ligand donates to the metal when forming a bond to the surface.

Nanocrystal surfaces are difficult to characterize due to both their spatial and temporal heterogeneity.[22, 38, 39] This problem is exacerbated by weak bonding on $CsPbX_3$ nanocrystal surfaces, which creates a highly dynamic ligand shell. Initial reports on $CsPbBr_3$ nanocrystals synthesized by the standard oleylamine/oleic acid protocol[10] have shown that a highly dynamic equilibrium exists between free and bound oleylammonium bromide ligand pairs while oleate

species do not bind to the surface.[40-42] Surface cesium can be replaced by the oleylammonium head group in a substitution mechanism.[41] Alternatively, oleylammonium can bind surface halides through an addition mechanism. The literature on surface passivation of lead halide perovskite materials is growing rapidly, with a wide variety of chemical species having been shown to improve photoluminescence.[3, 43-56] Here, we seek to unify these findings through a molecular-level understanding of surface trap passivation in $CsPbX_3$ nanocrystals; this requires a combined experimental and theoretical investigation of their surface chemistry.

In this article, we demonstrate a systematic route to highly luminescent $CsPbX_3$ nanocrystals with variable compositions and morphologies. We explore the relationship between surface chemistry and optoelectronic performance by performing a wide range of ligand exchanges. X-ray photoelectron spectroscopy, absolute photoluminescence quantum yield (PLQY) experiments, and *ab initio* calculations are used to elucidate the nature of the organic-inorganic interface and its role in charge trapping. The number of surface defects per nanocrystal is quantified by ^{1}H NMR spectroscopy and is consistent with a simple model of charge trapping. Surface halide vacancies are identified as the predominant source of charge trapping, with an effect that varies significantly based on $CsPbX_3$ halide composition. Different degrees of defect tolerance between the halide compositions helps to explain the relatively poor PLQY of $CsPbCl_3$ in addition to the high PLQY of $CsPbBr_3$ and $CsPbI_3$. Guided by *ab initio* calculations, we develop a general scheme for ligand passivation of deleterious under-coordinated lead atoms that is grounded in established principles of coordination chemistry. This analysis is used to prepare essentially trap-free $CsPbBr_3$ and $CsPbI_3$ nanocrystals along with brighter $CsPbBr_{3-x}Cl_x$ nanocrystals. We propose a general passivation mechanism whereby new ligands bind surface lead by substituting into surface halide vacancies, thus raising the energy of lead 6p levels to where they are no longer

present in the bandgap. This mechanism is able to unify existing literature reports, thereby informing synthetic and post-synthetic design principles for trap-free $CsPbX_3$ nanocrystals.

MATERIALS AND EXPERIMENTAL METHODS

Chemicals. Cesium carbonate (99.9%), 1-octadecene (90%), oleic acid (90%), oleylamine (70%), lead(II) bromide (99.999%), lead(II) chloride (99.999%), lead(II) iodide (99.999%), lead(II) oxide (99.999%), anhydrous toluene (99.8%), anhydrous ethyl acetate (99.8%), anhydrous hexanes (>99%), anhydrous tetrahydrofuran (>99%), didodecyldimethylammonium bromide (98%), mesitylene (>99.8%), benzoic acid (>99.5%), benzylamine (>99%), decylamine (95%), myristic acid (>99%), hexylphosphonic acid (95%), 2-ethyl-1-hexylamine (98%), fluoroacetic acid (95%), difluoroacetic acid (98%), trifluoroacetic acid (99%), methanesulfonic acid (>99%), tri-*n*-octylphosphine (97%), butyric acid (>99%), lead(II) nitrate (>99%), lead(II) hydroxide (99%), cesium acetate (>99.99%), toluene-d_8 (>99%), nickel(II) chloride hexahydrate (>97%), and zinc dust (>98%) were purchased from Sigma-Aldrich and used as received. Ethyliododifluoroacetate (96%) was purchased from Matrix Scientific and used as received. 2,2-difluorononanoic acid was synthesized from ethyliododifluoroacetate and 1-octadecene following a previously reported procedure.[57, 58]

Nanocrystal Synthesis and Isolation. $CsPbBr_3$ nanocrystals were synthesized following a previously reported procedure,[10] with slight modifications. Typically, anhydrous ODE (5 mL) and $PbBr_2$ (0.188 mmol) were loaded into a 3-neck flask inside of a glovebox, and the flask was then transferred to a Schlenk line and dried/degassed under vacuum at 110 °C for 15-20 minutes. Dried oleic acid (0.5 mL) and oleylamine (0.6 mL) were then injected under dry argon gas and the temperature was raised to 140 °C to complex the $PbBr_2$ salt. Following complete dissolution of $PbBr_2$, which we found to occur within 15-20 minutes, the temperature was raised to 155 °C in

preparation for the injection of warm (~100 °C) cesium oleate solution (0.5 mL, 0.125 M). Following injection, the mixture was stirred for 5 s and then cooled using an ice-water bath. Following the synthesis, 5-10 mL of anhydrous hexanes was added to the crude solution, which was then centrifuged at 4000 rpm for 3 min to remove excessively large nanocrystals and other unwanted byproducts. The supernatant was observed to be transparent and intensely green in color. The solubility of the nanocrystals depended on the relative proportions of ODE, a poor solvent for these nanocrystals, and hexanes, a better solvent. Hexanes was removed in a step-wise fashion by flushing the surface of the solution with a stream of argon or nitrogen, and different sizes of nanocrystals were isolated from the reaction mixture. Isolated nanocrystals were resuspended in anhydrous hexanes or toluene and stored in a glovebox.

Ligand Exchange Method. Stock solutions of nanocrystals (~1-2 μM) were precipitated with addition of an antisolvent (typically anhydrous ethyl acetate, 2× the volume of original nanocrystal solution), separated from the supernatant via centrifugation (10,000 rpm for 6 minutes), then resuspended in a dilute (~1-10 mM) mixture of new ligand pairs in anhydrous hexanes or toluene. Repeating this precipitation-resuspension process a total of 3 times was found to yield a complete exchange in all cases. Performing this process in neat solvent rather than a dilute ligand pair solution rapidly degrades the nanocrystals.

Optical Spectroscopy. All optical measurements were performed on dilute samples of nanocrystals in hexanes or toluene. For typical $CsPbBr_3$ nanocrystals, concentrations on the order of 1-10 nM were found to have suitable optical densities. Absorption spectra were collected on a Shimadzu UV-3600 spectrophotometer with 0.5 nm increments using the slowest scan speed. Photoluminescence emission spectra were collected on a Horiba Jobin Yvon TRIAX 320 Fluorolog. Time-resolved fluorescence lifetimes were collected on a Picoquant Fluotime 300 with

PMA 175 detector and an LDH-P-C-405 diode laser (excitation wavelength of 407.7 nm). Absolute quantum yields were determined optically using a custom integrating sphere spectrofluorometer which is described elsewhere.[59]

Powder X-ray diffraction (XRD). Diffraction patterns of drop-cast nanocrystal samples were obtained using a Bruker D-8 GADDS diffractometer equipped with a Co Kα source and a Bruker Vantec 500 detector. Patterns were typically collected by merging frames centered at 2θ = 30, 50, and 70 degrees where each frame was collected for 40 minutes.

X-ray Photoelectron Spectroscopy (XPS). XPS spectra of $CsPbBr_3$ nanocrystals drop-cast on a Si wafer were collected using Thermo Scientific K-Alpha Plus X-ray photoelectron spectrometer. The spectra were acquired with monochromatized Al Kα radiation and 400 μm beam size. Cs, Pb, and Br were quantified by fitting GL(30) peak shapes and calibrating the C 1s edge to 284.8 eV.

NMR spectroscopy. NMR spectra of micromolar concentrations of $CsPbBr_3$ nanocrystals in toluene-d_8 were measured on a Bruker 700 MHz spectrometer with an inverse cryoprobe for greatly enhanced ^1H sensitivity. Quantitative measurements were collected after tuning the probe and determining the exact 90° radio frequency pulse. After a spectrum was collected, concentration was determined by integrating the peak(s) of interest against an internal standard (mesitylene) of known concentration. 2D NOESY experiments were performed using a gradient-enhanced NOESY pulse sequence, with a mixing time of 500 ms and a delay time of 7 s. Spectra were typically collected overnight (10-12 hour acquisition times) to ensure high-quality data.

Computational Methods. Density functional theory calculations were performed using the Vienna *ab initio* simulation package (VASP).[60] The core−valence interaction was described by the projector−augmented wave (PAW) method.[61] The cutoff for planewave expansion was set to 300 eV. Structures were relaxed until the force on each atom was smaller than 0.05 eV/Å. For the

structural relaxation of systems with halide vacancies, the screened Coulomb hybrid functional of Heyd–Scuseria–Ernzerhof (HSE) was adopted,[62] and for the relaxation of other systems, the generalized gradient approximation of Perdew–Burke–Ernzerhof (GGA–PBE) was used.[63] The electronic structures for all systems considered were calculated at the HSE level after relaxation. The spin–orbit coupling (SOC) correction was also included in both structural relaxation and electronic structure calculations. The surface slab model was constructed based on orthorhombic $CsPbX_3$. It contains 11 atomic layers in a 2×2 supercell with 216 atoms. A vacuum layer larger than 12 Å was used to avoid interaction between periodic images. The Brillouin zone was sampled by the Γ point.

RESULTS AND DISCUSSION

On the Atomistic Nature of the $CsPbX_3$ Inorganic Surface. Following synthesis and isolation, colloidal $CsPbBr_3$ nanocrystals exhibit cube-like morphology with typical size distributions ±10% in edge length as measured (N=75 particles) by transmission electron microscopy (TEM) (See Supporting Information). Photoluminescence quantum yield (PLQY) values range from 60–90%, determined optically using an integrating sphere.[59] Although these nanocrystals are relatively bright, sub-unity PLQY values demonstrate the presence of energetic losses due to deleterious charge trapping and nonradiative recombination, thereby motivating an investigation into the origins of these processes. The underlying trapping pathways that prevent near-unity PLQY in $CsPbX_3$ nanocrystals remain a subject of debate, which hinders rational improvements of optoelectronic performance.

For metal chalcogenide nanocrystals, dangling bonds at the surface introduce localized mid-gap states that can trap charges.[21-23, 64, 65] However, *ab initio* calculations of pristine (100) $CsPbX_3$ surfaces terminated by CsX facets[19, 41, 66, 67] yield trap-free, fully delocalized electronic

structures without the need for passivating ligands (Figure S1).[19, 68] This suggests that surface dangling bond states of low-index CsX terminated $CsPbX_3$ nanocrystals lie outside of the bandgap and thus do not affect photoluminescence efficiency. Therefore, we hypothesized that as-synthesized surfaces are not pristine, but rather contain local point defects that are a likely cause of sub-unity PLQY in $CsPbX_3$ nanocrystals. Unfortunately, the atomistic nature of the $CsPbX_3$ nanocrystal surface remains poorly understood. As such, quantitative X-ray photoelectron spectroscopy (XPS) – a surface-sensitive technique – was used to elucidate the surface stoichiometry of four different $CsPbBr_3$ samples. Based on the inelastic mean free path, the first 2.0 nm of material was probed in this experiment. For these samples, each with PLQY of 60-65%, an average surface stoichiometry of Cs:Pb:Br of 0.78±0.04:1:2.83±0.02 was determined (Figure S2, Table S1). Deviations from the expected stoichiometry (Table S2-S3) support the hypothesis regarding the presence of surface point defects, namely vacancies in these systems.[18, 20, 69] However, the number of vacancies determined by XPS represents an upper bound, as the low cohesive energy of lead halide perovskite materials can lead to the loss of surface atoms when samples are transferred from the solvent phase to the vacuum, and exposed to high-energy X-rays in the ultra-high vacuum environment.[70, 71] In contrast, ambient techniques such as ^{1}H NMR spectroscopy can offer quantitative insight into surface structure without inducing sample evolution and/or degradation, as will be demonstrated later in this work.

Sub-stoichiometry of surface cesium is well-documented in the literature, and has been explained by a substitution mechanism where oleylammonium ions substitute into cesium vacancies.[41, 72, 73] A Pb:Br ratio that deviates from the expected stoichiometry is also well-documented in the literature, with the common interpretation being a lead-rich surface.[3, 51] However, this result can be equivalently interpreted as a bromide-deficient surface, an

interpretation that shapes the way we think about charge trapping in these materials. One can assess the validity of each interpretation by considering existing *ab initio* calculations of $APbX_3$ surface defects. For a lead-rich surface, extra lead atoms on CsX facets would need to occupy sites such as adatoms, antisites, and interstitials, which have prohibitively high (>2 eV) formation energies.[20, 68, 69] Additionally, a lead-rich surface introduces defect levels that are too deep (defined here as $>5k_bT$) within the bandgap to be consistent with 80-90% PLQY for as-synthesized $CsPbBr_3$ nanocrystals.[69] In contrast, a bromide-deficient surface would present bromide vacancies as the dominant defect type, which introduces shallow (defined here as $<5k_bT$) defect levels.[74-76] The presence of surface bromide vacancies is also consistent with labile oleylammonium bromide ligand pairs, bromide-poor synthetic conditions, and high anionic conductivities.[11, 12, 77, 78] Therefore, for both electronic and synthetic reasons, we believe that the 1:2.83±0.02 Pb:Br surface ratio can be accounted for with bromide vacancies rather than excess lead atoms.

The Role of Surface Halide Vacancies in Charge Trapping. Non-stoichiometric nanocrystal surfaces can harm optoelectronic performance by creating localized trap states.[65, 79-81] Guided by non-stoichiometric XPS results, halide-deficient surfaces were investigated as the potential source of charge trapping. We sought a method for controlling the introduction of halide vacancies on the surface of $CsPbX_3$ nanocrystals. Given the unstable nature of lead halide perovskite materials, it was particularly important to devise a method that can remove surface halides without altering or degrading the material in any other way. This was achieved by directly exploiting the weak bonding of oleylammonium halide ligand pairs, whose chemical equilibrium is described by eq 1. V_X represents a surface halide vacancy.

$$RNH_3{}^+X^- + CsPbX_3 \cdot V_X \leftrightarrow CsPbX_3 \cdot RNH_3{}^+X^- \quad (1)$$

It is unfavorable for oleylammonium ions to dissociate as discrete solvated ions in low polarity solvents such as toluene, therefore they are most likely removed from the surface with a counterion to preserve charge neutrality.[82] With oleate ions absent from the surface,[40-42] halide ions are the only available counterions present. A simple dilution experiment offers a very mild and controllable way to introduce surface halide vacancies as the ligand pair equilibrium shifts towards free species. As such, monitoring the PLQY over a range of concentrations offers direct insight into the PLQY dependency on the halide vacancy concentration. Although reabsorption can be a concern when high concentrations are present in a fluorescence experiment, this would result in measured PLQY being lower than true PLQY, which would cause measured PLQY to decrease with increasing concentration. However, the opposite trend was observed for these samples, indicating that the effects of halide vacancies dominate over any reabsorption that may be present. Although excessive dilution can induce rapid degradation of $CsPbX_3$ nanocrystals, this was only found to occur for nanocrystal concentrations <0.005 μM, which is far below the concentrations utilized here.

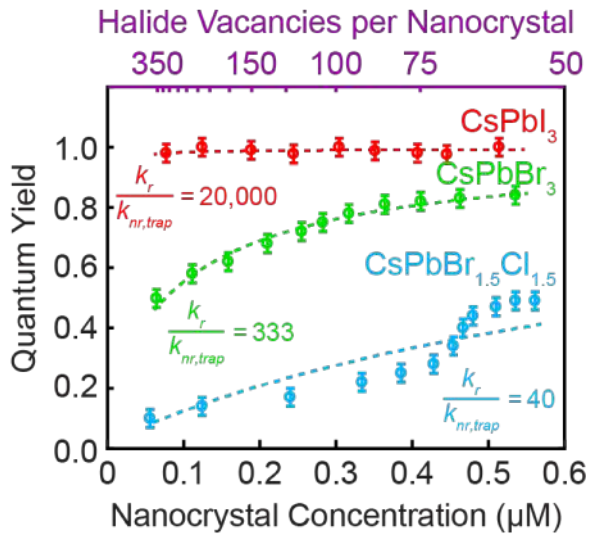

Figure 1. Absolute PLQY as a function of nanocrystal concentration for $CsPbBr_{1.5}Cl_{1.5}$, $CsPbBr_3$, and $CsPbI_3$. Nanocrystal concentration and surface halide vacancy concentration are inversely related due to weak binding of oleylammonium halide ligand pairs. This allows the relationship between PLQY and halide vacancy concentration to be investigated. Surface halide vacancies are observed to have a negligible effect on $CsPbI_3$ nanocrystals, a moderate effect on $CsPbBr_3$ nanocrystals, and a significant effect on $CsPbBr_{1.5}Cl_{1.5}$ nanocrystals. The data can be fit with a simple trapping model, which offers insight into the relative defect tolerance of each material by allowing the determination of $k_r/k_{nr,trap}$.

These experiments demonstrate a composition-dependent relationship between surface halide vacancy concentration and PLQY. Increasing the concentration of surface halide vacancies

is observed to have a negligible effect on $CsPbI_3$, a small to moderate effect on $CsPbBr_3$, and a significant effect on $CsPbBr_{1.5}Cl_{1.5}$, as shown in Figure 1. We did not investigate pure $CsPbCl_3$ due to instrument limitations at the $CsPbCl_3$ bandgap, but we find homogenous $CsPbBr_{3-x}Cl_x$ alloys[83] to be a suitable substitute for examining PLQY as a function of halide composition. Although $CsPbI_3$ nanocrystal photophysics appear unchanged upon dilution, ^{1}H NMR spectroscopy experiments were used to confirm that dilution does in fact result in significant ligand pair desorption. The oleylammonium iodide ^{1}H NMR linewidth decreased significantly as the sample was diluted (Figure S3). The linewidth of a ligand pair in fast exchange is a population-weighted average of free and bound signals,[84] as described by eq 2:

$$\lambda_{obs} = \frac{N_{free}}{N_{total}}\lambda_{free} + \frac{N_{bound}}{N_{total}}\lambda_{bound} \quad (2)$$

where λ is the linewidth and N is the number of ligand pairs per nanocrystal. N_{total}, λ_{free}, and λ_{bound} are unchanged by dilution, therefore a narrowing of the observed linewidth must be caused by a decrease in N_{bound} and a concomitant increase in N_{free}. This directly demonstrates that the equilibrium in eq 1 is shifting towards free species in these experiments.

The plot of PLQY vs. nanocrystal concentration was analyzed within the context of a simple trapping model, eq 3-4.

$$PLQY = 1 - \frac{N_{trap}}{\frac{k_r}{k_{nr,trap}} + N_{trap}}, \quad (3)$$

$$N_{trap} = \frac{N_{max}}{1 + K_{eq}[RNH_3{}^+X^-]} \quad (4)$$

where k_r is the radiative rate, $k_{nr,trap}$ is the effective nonradiative rate per trap, N_{trap} is the number of surface traps per nanocrystal, N_{max} is the maximum number of surface traps per nanocrystal, K_{eq} is the free vs. bound equilibrium constant for oleylammonium halide ligand pairs, and $[RNH_3^+X^-]$ is the concentration of oleylammonium halide ligands pairs free in solution. The determination of all variables other than k_r and $k_{nr,trap}$ (Figure S4) leaves $k_r/k_{nr,trap}$ as the sole fitting parameter. This model offers close fits for $CsPbBr_3$ and $CsPbI_3$, and although it fails to accurately capture the complex sigmoidal shape of the $CsPbBr_{1.5}Cl_{1.5}$ data, valuable insight into the underlying photophysics of these systems can still be gained. It should be noted that this sigmoidal shape is similar in nature to the dramatic step-like decrease in PLQY that was observed during the displacement of cadmium carboxylate complexes from the surface of cadmium selenide nanocrystals.[64] These observations suggest that in the mixed halide case there appears to be a cooperative effect in ligand dissociation, and highlight the need for additional investigations of the relationship between nanocrystal surface structure and optical properties.[22]

Defect tolerance, which we define here as arising through very large values of $k_r/k_{nr,trap}$, varies significantly between the different halide compositions (Figure 1). $k_r/k_{nr,trap} = 20{,}000$ allows $CsPbI_3$ nanocrystals to maintain near-unity PLQY despite the presence of several hundred surface halide vacancies. Within the lead halide perovskite family, the iodide materials appear to be the closest to defect impervious. $k_r/k_{nr,trap} = 333$ for $CsPbBr_3$ nanocrystals indicates these materials are also relatively tolerant of defects, although the effects of surface halide vacancies clearly cannot be ignored in this system. $k_r/k_{nr,trap} = 40$ for $CsPbBr_{1.5}Cl_{1.5}$ nanocrystals is the most analogous to defect-intolerant metal chalcogenide nanocrystals, where even a small number (<5% of the surface) of traps will yield PLQY values <20%. As a final comment in support of halide-deficient

surfaces, it should be noted that if under-coordinated lead in a form other than that created by halide vacancies was the predominant source of charge trapping, no variation in $k_r/k_{nr,trap}$ and PLQY between different halide compositions would be expected. *Ab initio* calculations have shown that these defects form deep mid-gap states that would affect all halide compositions equally.[69]

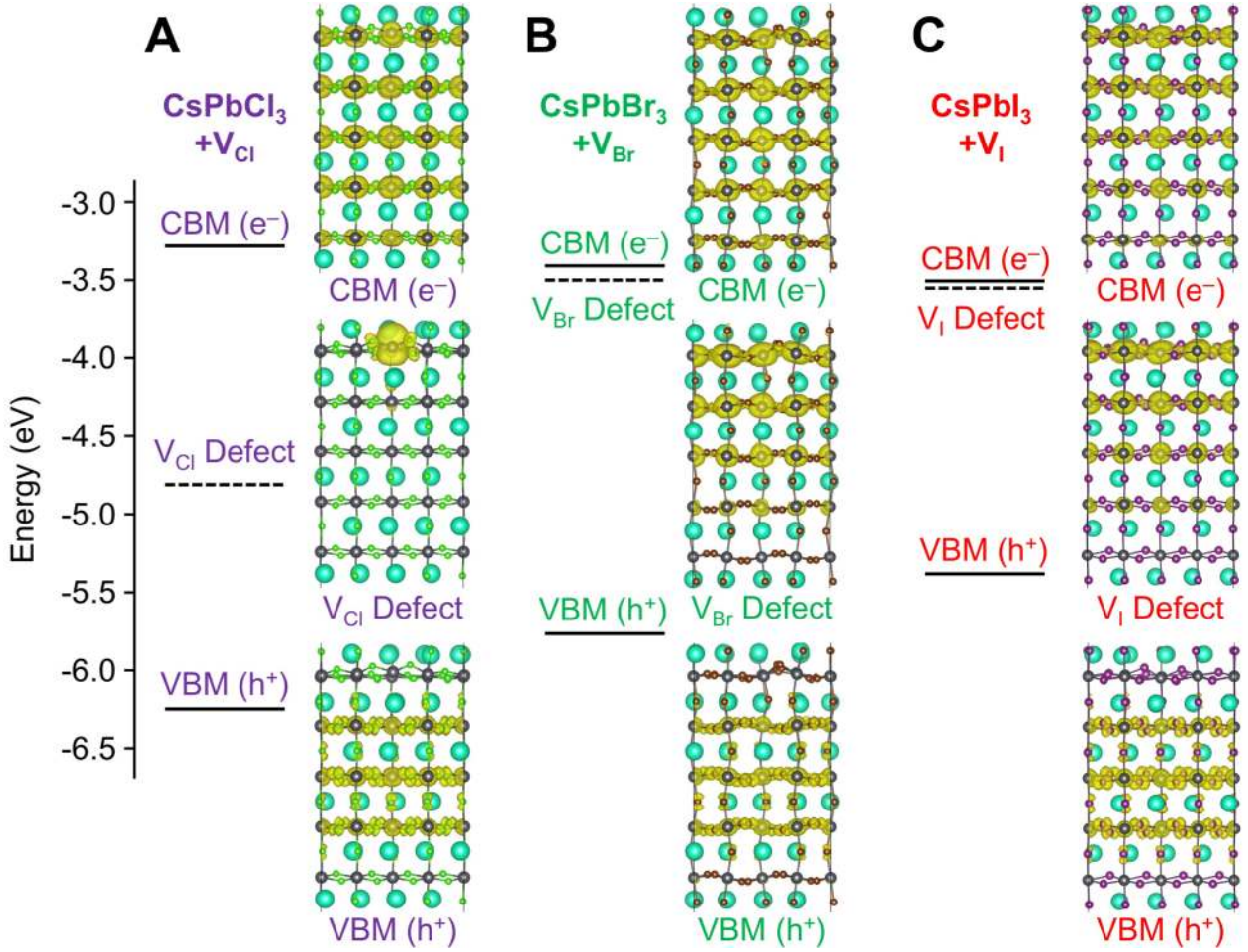

Figure 2. Electronic structure and charge density calculations at the HSE+SOC level of theory for (A) $CsPbCl_3$ with a surface chloride vacancy ($CsPbCl_3+V_{Cl}$), (B) $CsPbBr_3$ with a surface bromide vacancy ($CsPbBr_3+V_{Br}$), and (C) $CsPbI_3$ with a surface iodide vacancy ($CsPbI_3+V_I$). The top surface of the crystal slab is halide-deficient while the bottom surface is pristine. Absolute CBM energies are set according to electrochemically measured values, and relative energies are given by the calculations. Cs, Pb, Cl, Br, and I atoms are shown as blue-green, gray, green, orange, and purple, respectively.

***Ab Initio* Calculations of Halide-Deficient $CsPbX_3$ Surfaces.** *Ab initio* calculations were used to further investigate halide-deficient surfaces as the suspected source of charge trapping. A single

halide vacancy (V_{Cl}, V_{Br}, or V_I) was created on the surface of each crystal slab to model a halide-deficient surface. Native oleylammonium surface ligands are excluded because pristine $CsPbX_3$ crystals terminated by CsX facets exhibit fully delocalized, trap-free band structures without the need for passivating ligands (Figure S1). As such, differences in electronic structure between pristine and halide-deficient surfaces can be directly attributed to surface halide vacancies.

$CsPbCl_3$+V_{Cl} is readily recognized as a three-level system, with a highly localized trap state deep within the bandgap in addition to the fully delocalized valence band maximum (VBM) and conduction band minimum (CBM), as shown in Figure 2A. The mid-gap state exhibits significant atomic character; ~80% of this state is comprised of 6p orbitals of the lead atom that is left under-coordinated by the surface chloride vacancy. $CsPbBr_3$+V_{Br} and $CsPbI_3$+V_I also appear as three-level systems (Figure 2B-C). However, the nature of the mid-gap defect levels differs significantly from the defect level in $CsPbCl_3$+V_{Cl}. Rather than being highly localized and deep within the bandgap, these states are shallow and only weakly localized towards the halide-deficient surface. In these two systems, the under-coordinated lead atoms only contribute ~3% to the defect states. It should be noted that the HSE+SOC level of theory is required to observe the shallow levels in $CsPbBr_3$+V_{Br} and $CsPbI_3$+V_I.[85, 86] Calculations with GGA–PBE+SOC, which underestimated the bandgap by ~1 eV,[87] produced nominally trap-free systems (Figure S5). However, sub-unity experimental PLQY values indicate that these systems are not trap-free.

It is particularly insightful to interpret these calculations of halide-deficient $CsPbX_3$ surfaces in light of experimental results. The calculated position of these defect levels relative to the CBM is highly consistent with the $k_r/k_{nr,trap}$ ratios determined in Figure 1. Nanocrystals can sustain a high charge transfer rate at high driving force,[88] and with the $CsPbCl_3$+V_{Cl} defect state located directly in the middle of the bandgap, efficient trapping of charges would be expected.[89]

Additionally, the highly localized nature of this mid-gap state should result in significant nonradiative recombination, thereby yielding a relatively low $k_r/k_{nr,trap}$ as well as relatively poor PLQY values for $CsPbCl_3$ nanocrystals. In contrast to highly localized charges in $CsPbCl_3$+V_{Cl}, these calculations suggest that electrons in halide-deficient $CsPbBr_3$ and $CsPbI_3$ are only weakly localized while holes remain fully delocalized, and thus trap-assisted nonradiative recombination is therefore expected to be relatively ineffective in $CsPbBr_3$ and $CsPbI_3$.[90-92] This allows $k_r/k_{nr,trap}$ to become quite large in these two systems, even though k_r is decreased relative to $CsPbCl_3$.[10, 93]

We sought to use *ab initio* calculations not only to investigate the predominant source of charge trapping, but also to identify a potential surface passivation mechanism. Oleate was investigated as a passivating ligand, as it has the potential to bind the under-coordinated lead atoms that have been implicated in charge trapping. X-type CH_3COO^- moieties, truncated computational models for oleate, were substituted into surface halide vacancies of the structures studied in Figure 2. These structures produce trap-free bandgaps with fully delocalized VBM and CBM states for each halide composition, indicating that anionic surface ligands can effectively alter the energetics of lead-based defect levels, removing them from within the bandgap (Figure 3). However, several reports have demonstrated that oleate is not present on the surface of as-synthesized $CsPbBr_3$ nanocrystals,[40-42] which we ascribe to a hard-soft mismatch between hard carboxylates and soft lead binding sites.[22, 94] This motivates a search for new, softer ligands that can bind deleterious under-coordinated lead.

A Versatile Ligand Exchange and Purification Method. Investigations into the effects of new ligand shells would be greatly enhanced by a versatile ligand exchange method.[64, 95] However, to the best of our knowledge, no versatile colloidal ligand exchange method has yet been reported for $CsPbX_3$ nanocrystals. As such, precise manipulations of $CsPbX_3$ nanocrystal surfaces and entire

ligand shells are not readily available. Here, we introduce a colloidal ligand exchange method that can exchange native oleylammonium halide ligand pairs for a mixture of alkylammonium halide and alkylammonium-alkylcarboxylate/alkylphosphonate ligand pairs (Figure S6). This is

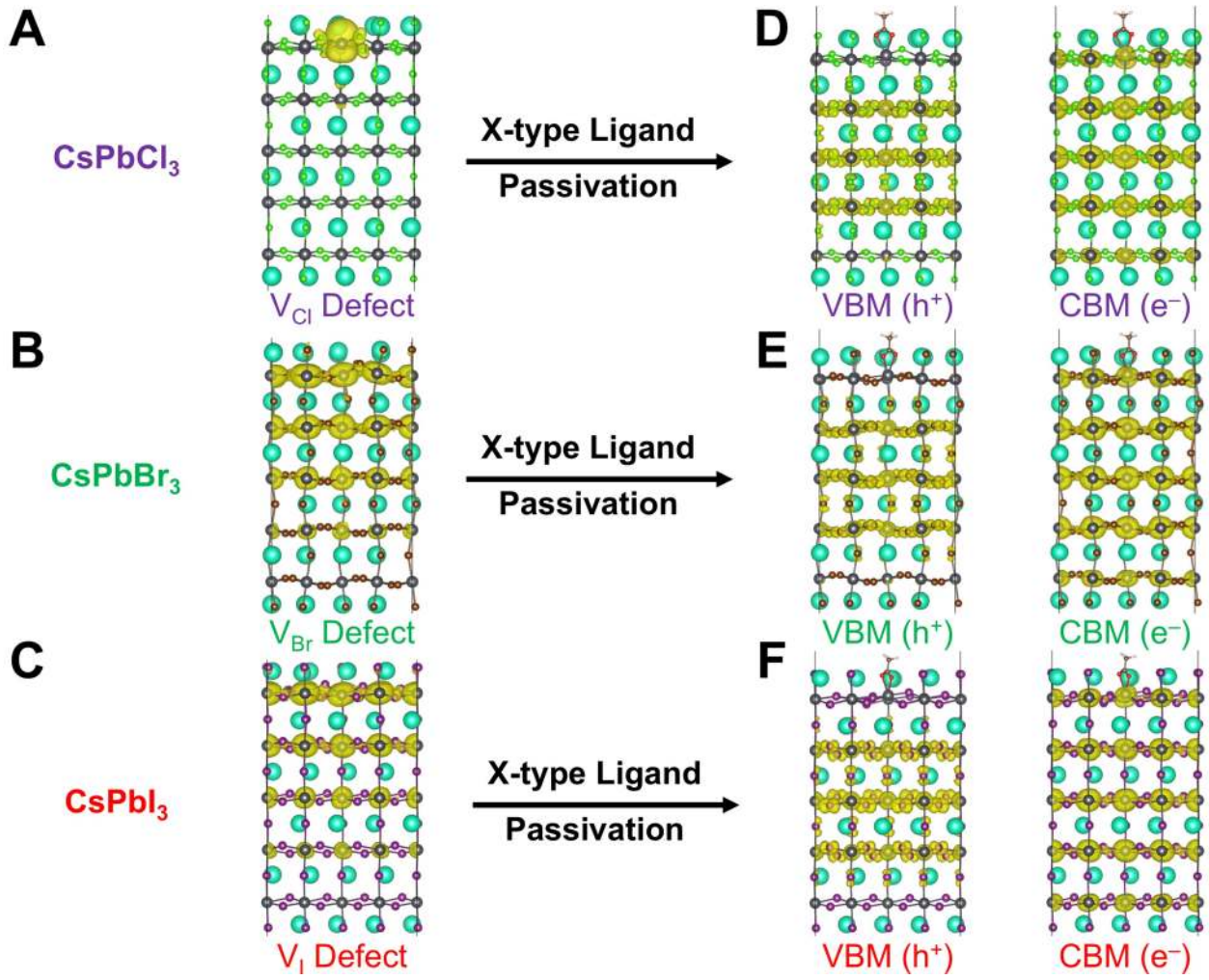

Figure 3. Charge density calculations at the HSE+SOC level of theory for (A) $CsPbCl_3$ with a surface chloride vacancy ($CsPbCl_3+V_{Cl}$), (B) $CsPbBr_3$ with a surface bromide vacancy ($CsPbBr_3+V_{Br}$), (C) $CsPbI_3$ with a surface iodide vacancy ($CsPbI_3+V_I$), (D) $CsPbCl_3+V_{Cl}$ from (A) with a CH_3COO^- X-type passivating ligand, (E) $CsPbBr_3+V_{Br}$ from (B) with a CH_3COO^- X-type passivating ligand, (F) $CsPbI_3+V_I$ from (C) with a CH_3COO^- X-type passivating ligand. VBM and CBM states are unaffected by surface halide vacancies in (A), (B), and (C), and thus are excluded. In all cases, X-type passivation of halide-deficient surfaces yields a trap-free bandgap with fully delocalized VBM and CBM states. Cs, Pb, Cl, Br, I, O, C, and H atoms are shown as blue-green, gray, green, orange, purple, red, brown, and white, respectively.

accomplished by directly exploiting the weak bonding between native ligand pairs and the $CsPbX_3$ surface (Figure S7). Stock solutions of nanocrystals (~1-2 μM) are precipitated with the addition of antisolvent, separated from the supernatant via centrifugation, and resuspended in ~1-10 mM

solutions of new ligand pairs. Given the ionicity of perovskite nanocrystals, the use of molecular combinations that can form ion pairs is highly beneficial. Performing this exchange process on $CsPbBr_3$ nanocrystals with a dilute solution of alkylamine or alkylcarboxylic/alkylphosphonic acid alone, but not both species, yielded a weakly fluorescent, off-white precipitate. X-ray diffraction determined the precipitate to be comprised primarily of CsBr and Cs_4PbBr_6 phases (Figure S8).

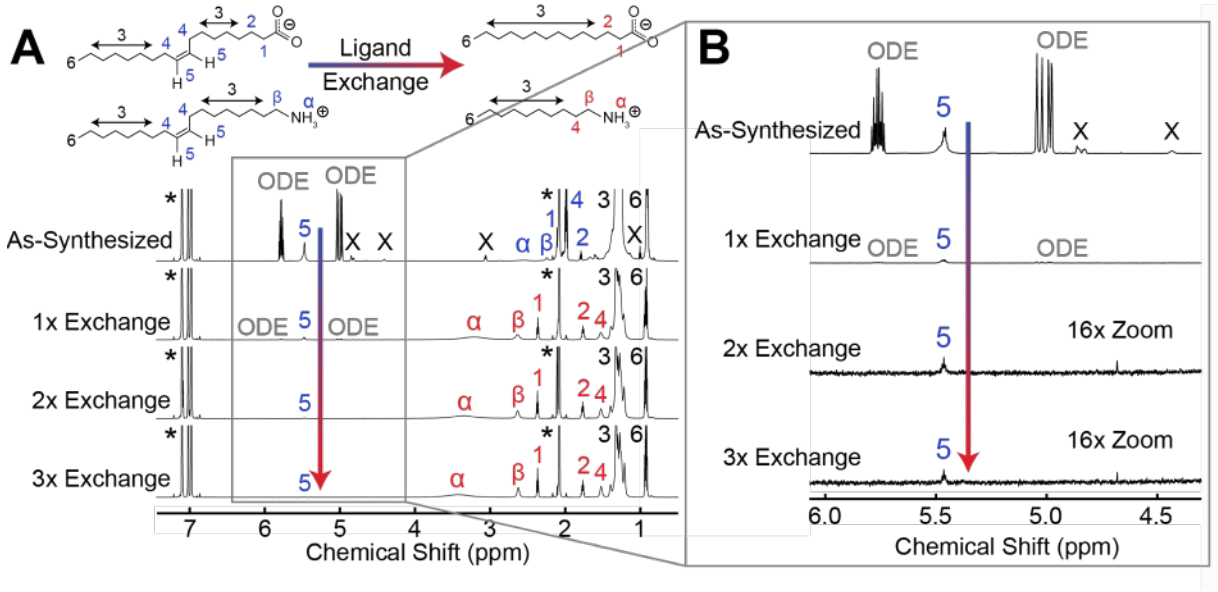

Figure 4. (A) ^{1}H NMR spectra for each step of a ligand exchange from native (blue) unsaturated ligand pairs (oleylammonium and oleate) to new (red) saturated ligand pairs (decylammonium and myristate). Resonances denoted by X are impurities. Concentration of $CsPbBr_3$ nanocrystals: 1.6 μM in toluene-d_8. (B) The 4-6 ppm region of interest from (A). This region contains resonances from native oleyl vinyl protons (5), 1-octadecene (ODE), and unknown impurities (X). All native species are reduced to <0.5% of their original concentration, demonstrating a complete ligand exchange.

To gain insight into the step-by-step evolution of this method, an exchange from as-synthesized, unsaturated ligand pairs (oleylammonium and oleate) to saturated ligand pairs (decylammonium and myristate) was studied via quantitative ^{1}H NMR for $CsPbBr_3$ nanocrystals (Figure 4, Figure S9). Unsaturated ligand pairs and 1-octadecene (ODE) both have alkene resonances in the 4-6 ppm range, which are useful for quantitative studies since they are located downfield from the many overlapping alkyl resonances in the 0-3 ppm region. Exchanging for saturated ligand pairs, which have no alkene resonances, allows the region of interest to be studied

for the removal of alkene-containing species, all of which should be removed to constitute a complete ligand exchange and purification (Figure 4B).

The exchange is observed to reach >99% exchange after three precipitation and resuspension steps, i.e. three exchange cycles. Appearance of decylammonium and myristate resonances and disappearance of alkene resonances confirms that native unsaturated ligand pairs are exchanged for non-native saturated ligand pairs (Figure 4). All native organic species being reduced to <0.5% of their original concentration confirms a complete ligand exchange. This is explicitly demonstrated by exchanging to ligand pairs such as benzylammonium-oleate, oleylammonium-benzoate, and oleylammonium-difluoroacetate, which have spectrally isolated resonances that grow in downfield of the overlapping alkyl region as the exchange progresses (Figure S10-S12). Each of these resonances shows a broadened peak that is characteristic of interaction with nanocrystal surfaces.[36, 64, 88, 96]

This exchange method also serves to purify nanocrystals of ODE, impurities, and synthesis byproducts such as lead oleate (Figure S13). As such, a resuspension solution of dilute oleylamine and oleic acid can be used to purify as-synthesized nanocrystals without compromising high PLQY or colloidal stability. X-ray diffraction, absorbance, photoluminescence, TEM, and integrating sphere PLQY measurements confirm that the inorganic nanocrystalline core remains unchanged, indicating that purification induces no macroscopic changes to the ensemble of particles (Figures S14-S16).

Softer Lewis Bases Bind to Nanocrystal Surface. With control over entire ligand shells established, new passivating ligand pairs were investigated. In light of the proposed hard-soft

mismatch between hard oleate and soft lead, softer carboxylates were targeted by exploring tail groups that decrease electron density on the binding head (Figure S17, Table S5). This can be accomplished through resonance and/or induction.[97, 98] Following a ligand exchange to

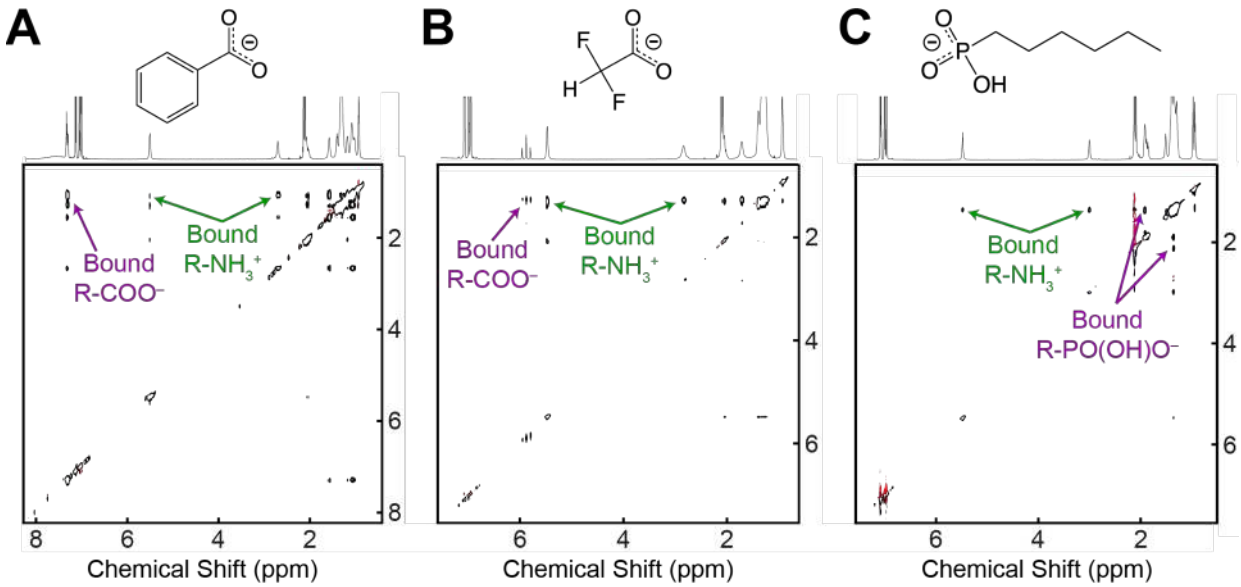

Figure 5. ^{1}H NOESY NMR spectra of $CsPbBr_3$ nanocrystal samples exchanged to ligand pairs of oleylammonium and (A) benzoate, (B) difluoroacetate, and (C) hexylphosphonate. All ligand pairs feature negative (black) NOE signals rather than positive (red) NOE signals, thereby corroborating their interaction with the nanocrystal surface. A small amount of red coloring is also present, but this is due to t1 noise rather than a positive NOE signal.

oleylammonium–R-COO$^-$ pairs, where R-COO$^-$ is benzoate, fluoroacetate, and difluoroacetate, Nuclear Overhauser Effect (NOESY) NMR spectroscopy confirms that these softer carboxylates bind to the nanocrystal together with oleylammonium (Figure 5A-5B). Each ligand pair features negative (black) cross peaks in the presence of nanocrystals, in contrast to positive (red) cross peaks when no nanocrystals are present (Figure S18).[40, 99] A change in the sign of the cross peak demonstrates that the tumbling frequency of these ligand pairs decreases significantly in the presence of nanocrystals, thereby confirming their interaction with the nanocrystal surface.[100] By utilizing the tail group to modulate electron density on the binding group, one can selectively coordinate or dissociate carboxylates in this system. The affinity of softer X-type ligands for the nanocrystal surface is further supported by the negative (black) NOE of oleylammonium-

hexylphosphonate (Figure 5C, Figure S19), which corroborates binding of these ligand pairs.[101] Although X-type Lewis bases such as these could presumably also bind to surface cesium, this is thermodynamically unfavorable,[41] and therefore these new anionic ligands are likely binding entirely to surface lead by substituting into halide vacancies. Experimental evidence in support of this was provided by additional ^{1}H NMR and optical experiments (*vide infra*).

Analysis of the NMR linewidth of new surface-bound carboxylates provides valuable evidence for lead as the binding site for these ligands. Eq 2 can be rearranged to solve for the number of bound ligands:

$$N_{bound} = N_{total}\left(\frac{\lambda_{obs} - \lambda_{free}}{\lambda_{bound} - \lambda_{free}}\right) \quad (5)$$

By preparing purified samples at the upper limits of colloidal stability so that an initially saturated nanocrystal surface can be assumed, λ_{bound} was determined to be 290±30 Hz for protons directly adjacent to the binding head (Figure S20). A saturated solution of the same nanocrystals following a ligand exchange to oleylammonium-difluoroacetate pairs displayed a linewidth of 10.7±0.2 Hz for the difluoroacetate proton, which corresponds to the formation of 180±20 new lead–difluoroacetate bonds for a fully passivated surface. The determination of 180±20 new bonds to lead is supported by the simple trapping model used in Figure 1. These $CsPbBr_3$ nanocrystals, which displayed a PLQY value of 62±3% before the ligand exchange, are expected to have 190±20 surface halide vacancies. These values indicate that new anionic X-type ligands access ~12% of the nanocrystal surface, which is in close agreement with a previous report from our group.[3]

Anionic X-type Ligands Can Produce Essentially Trap-Free Surfaces. *Ab initio* calculations suggested that formation of new lead–ligand bonds is expected to be accompanied by a significant

increase in optoelectronic performance. As such, the effect of softer, X-type ligands on photoluminescence was investigated. Moderate 60-65% PLQY $CsPbBr_3$ nanocrystals were selected to maximize the presence of under-coordinated lead atoms. A fraction was exchanged with an oleylammonium-hexylphosphonate solution using the method described above, and a

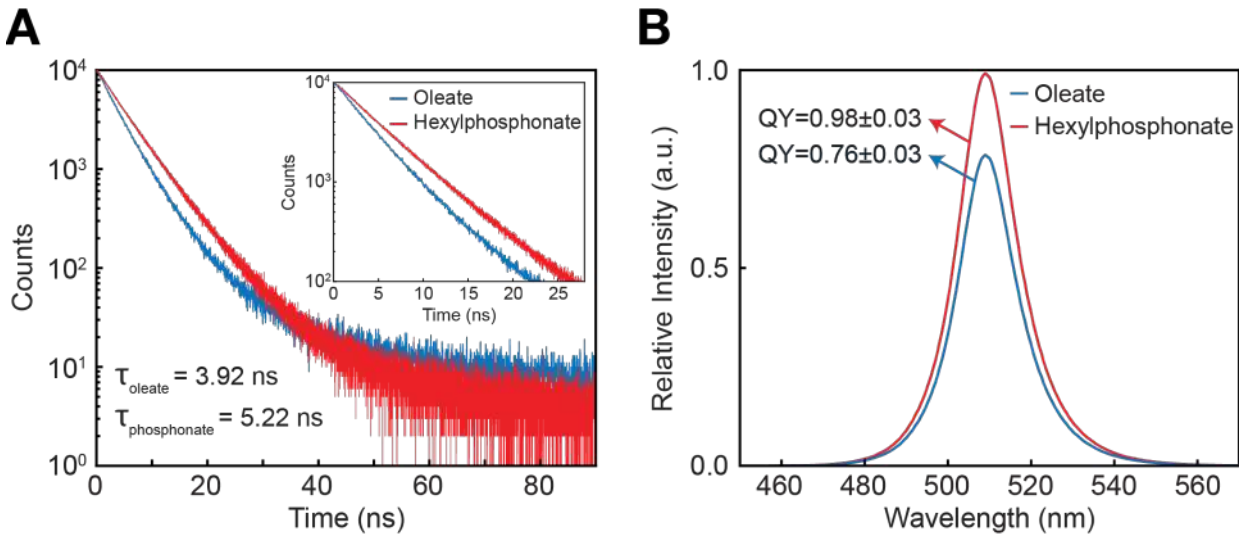

Figure 6. (A) Time-resolved photoluminescence lifetimes under pulsed 407.7 nm excitation (10 MHz) at room temperature for $CsPbBr_3$ nanocrystal samples in hexanes. Samples were exchanged to identical concentrations of oleylammonium-oleate (blue) and oleylammonium-hexylphosphonate (red). (B) Normalized steady-state photoluminescence spectra and absolute PLQY values for the same samples as in (A) under 437 nm excitation in hexanes. Nanocrystal and ligand pair concentration are identical for samples compared in (A) and (B), which is required for a meaningful PLQY comparison (Figure S21).

second fraction was purified with an oleylammonium-oleate solution of identical concentration as a control. Excited state lifetimes under 407 nm pulsed excitation are shown in Figure 6A. Lifetime values were determined by fitting each decay curve to a single-exponential over the first two decades. The purified oleylammonium-oleate sample (blue) shows a decay characteristic of an emitter with a distribution of trap states,[25, 32, 102-104] whereas the oleylammonium-hexylphosphonate exchanged sample (red) shows a decay that closely resembles that of a two-level emitter, indicating that deleterious trap states are almost completely passivated. Removal of trap states should be accompanied by a significant increase in PLQY, which was confirmed by integrating sphere measurements of PLQY=0.76±0.03 for oleylammonium-oleate (blue) and

PLQY=0.98±0.03 for oleylammonium-hexylphosphonate (red), as shown in Figure 6B. Both samples were prepared with 4 ligand pairs per available binding site and measured at a nanocrystal concentration of 0.1 μM; identical nanocrystal and ligand pair concentrations are required for a meaningful PLQY comparison (Figure S21). Importantly, the demonstration of near-unity PLQY in $CsPbBr_3$ nanocrystals is not unique to hexylphosphonate. We demonstrate significantly improved photoluminescence with a wide variety of chemical functionalities, including fluorinated carboxylates, sulfonates, and phosphines (Figure S22-S23).

We have focused entirely on the coordination chemistry between surface lead and passivating ligands to explain the coordination and dissociation of various species, but solubility may also play a role. For example, small fluorinated carboxylates will be less soluble in toluene than oleate and therefore could be driven to the surface by solubility effects rather than binding affinity for surface lead. To address this issue directly, a long chain analogue to difluoroacetic acid was synthesized, namely 2,2-difluorononanoic acid. In an optical comparison between oleylammonium-difluoroacetate and oleylammonium-2,2-difluorononanoate, both ligand pairs were observed to increase $CsPbBr_3$ PLQY by ~120% (Figure S24). No significant difference in surface passivation is observed at lower concentrations, indicating that solubility plays a minimal role. At higher concentrations, difluoroacetate yields a slightly higher PLQY, indicating that the long alkyl chain of 2,2-difluorononanoate hinders packing efficiency as coverage of the nanocrystal surface approaches saturation.

This demonstration of X-type ligand pairs as effective passivating ligands for $CsPbBr_3$ nanocrystals stands in contrast to metal chalcogenide nanocrystals, where Z-type ligands such as $Cd(O_2CR)_2$ have been shown to play a critical role in surface passivation.[21, 64] In our exploration of Z-type ligands for $CsPbBr_3$ nanocrystals, namely lead oleate, we observed a negative effect on

PLQY (Figure S25) that is consistent with our arguments about under-coordinated surface lead. Although this is not an exhaustive study of $CsPbX_3$ Z-type ligands, this result indicates that while the well-developed toolbox for metal chalcogenide nanocrystals can be readily applied to $CsPbX_3$ nanocrystals, differences in the nature of the bonding dictate different surface modification strategies.

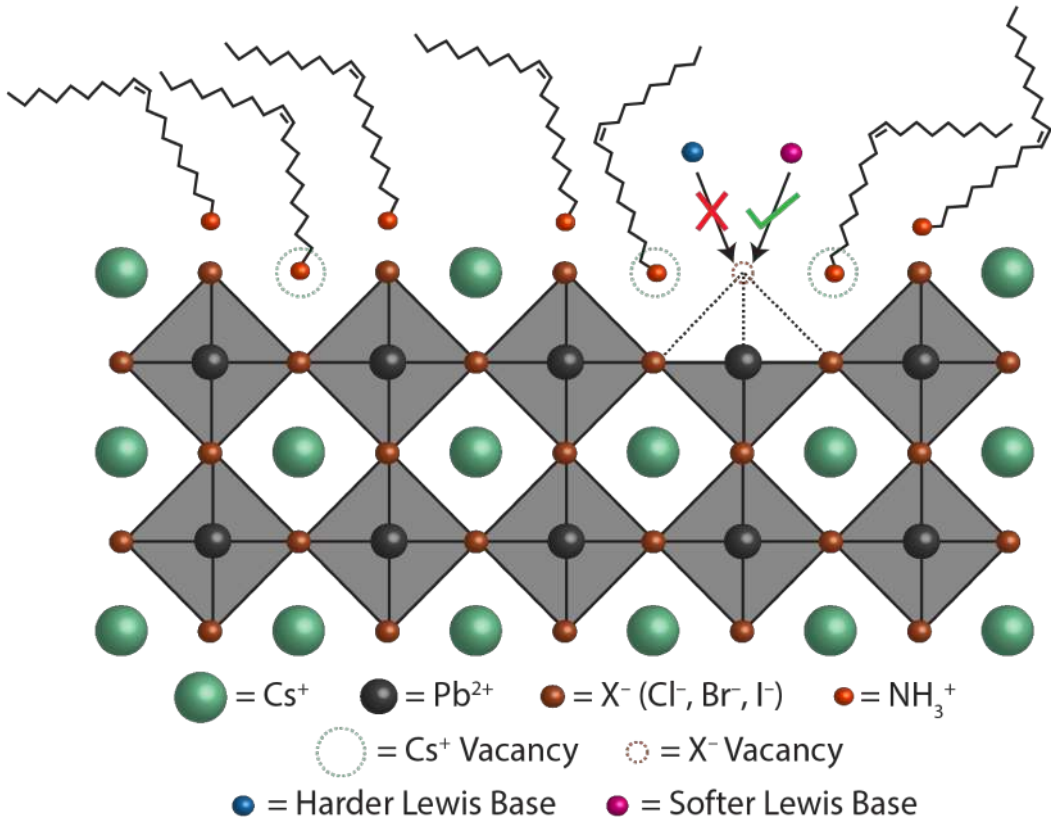

Figure 7. Schematic representation of a cesium- and halide-deficient surface terminated by CsX facets, consistent with experimental results. Approximately half of surface cesium is substituted by oleylammonium ions, and ~12% of surface halide sites are vacant. Halide vacancies create under-coordinated lead atoms, which can either be left unpassivated or passivated depending on the hardness or softness of the Lewis base that is available to coordinate lead.

A General Mechanism for $CsPbX_3$ Surface Passivation. $CsPbX_3$ nanocrystals spontaneously move towards simple cubic shapes with nearly perfect low-index CsX facets. The healing of point defects on these surfaces is essential for the realization of trap-free $CsPbX_3$ nanocrystals. Despite a growing body of literature on surface passivation of lead halide perovskite materials, a general understanding that can unify these reports does not yet exist. We propose that these findings can

all be explained by the mechanism we present here. Lewis bases, which can be ionic halide sources such as quaternary ammonium bromide salts or CH_3NH_3Br,[47, 54] neutral molecules such as thiophene or pyridine,[53] or anionic X-type ligands such as alkylphosphonates or S^{2-},[45, 52] substitute into surface halide vacancies and bind under-coordinated lead. These ligands raise the energy of lead 6p states to where they are no longer energetically accessible by photoexcited electrons in the conduction band, thereby increasing optoelectronic performance. This general surface passivation mechanism is depicted schematically in Figure 7. The crystal terminates with the CsX facet, with both cesium and halide vacancies present. Halide vacancies expose underlying lead atoms, which can be unpassivated or passivated depending on the hardness of softness of the X-type Lewis base that is present.

Proposed Design Principles for Trap-Free $CsPbX_3$ Nanocrystals. Knowledge of $CsPbX_3$ surface chemistry and its role in charge trapping can be used to propose design principles for the preparation of trap-free $CsPbX_3$ nanocrystals. With strong evidence for surface halide vacancies as the predominant source of charge trapping, design principles should focus on eliminating the presence and/or effects of these defects.

Synthetic control over the surface halide vacancy concentration can be achieved by exploring alternative precursors to lead halide salts, which are intrinsically halide-deficient relative to the final $CsPbX_3$ nanocrystalline product. We find a recent report that decouples lead and halide stoichiometry by employing benzoyl halide precursors to be particularly promising.[105] When synthesizing $CsPbCl_3$, weak (PLQY <10%) luminescence was observed for a stoichiometric injection of chloride precursor, which stands in stark contrast to a record high PLQY of ~65% when an excess of chloride precursor was injected. XPS determined the highest X:Pb ratio for the product of this synthesis, suggesting that excess halide precursor can increase PLQY by

Table 1. Effect of Various Chemical Functionalities on $CsPbX_3$ Nanocrystal PLQY

Significant Improvement of PLQY	Negligible/Negative Effect on PLQY
Hexylphosphonate (oleylammonium)	Oleate (oleylammonium)
Benzoate (oleylammonium)	Butyrate (oleylammonium)
Fluoroacetate (oleylammonium)	Acetate (oleylammonium)
Difluoroacetate (oleylammonium)	Carbonate (cesium)
Trifluoroacetate (oleylammonium)	Nitrate (lead)
2,2-difluorononanoate (oleylammonium)	Lead oleate (none)
Methanesulfonate (oleylammonium)	Hydroxide (lead)
Trioctylphosphine (none)	Acetate (cesium)

minimizing surface halide vacancy concentrations.[49] From a post-synthetic perspective, we have demonstrated the importance of coordination chemistry in designing the optimal passivating ligand shell for $CsPbX_3$ nanocrystals. Under-coordinated lead atoms are the predominant source of charge trapping, and with lead as a relatively soft Lewis acid, the hardness or softness of Lewis bases must also be considered. Harder species such as alkylcarboxylates, carbonates, and nitrates are ineffective passivating ligands, while softer species such as alkylphosphonates, fluorinated carboxylates, and sulfonates were found to be effective passivating ligands, as summarized in Table 1 with the relevant counterion in parentheses. In summary, synthetic design of trap-free $CsPbX_3$ nanocrystals should include decoupled tunability of cesium, lead, and halide precursors, and post-synthetic design of ligand shells should employ ionic X-type Lewis acid-base pairs, where the softness of the Lewis base is well-matched to the softness of under-coordinated lead in the nanocrystal.

While the work presented here has focused entirely on $CsPbX_3$ nanocubes, we expect these findings to extend to nanoplates, nanowires, and other morphologies. Indeed, experiments on nanoplates and nanowires demonstrate similar trends, namely PLQY that is lowest in $CsPbCl_3$ and highest in $CsPbI_3$ (Figure S26), as well as significant increases in PLQY of $CsPbBr_3$ materials when softer, X-type Lewis bases are employed. This work provides a rational framework for

highly luminescent lead halide perovskite nanocrystals of variable compositions and dimensionalities, which we anticipate will increase the performance of these materials in photonic and optoelectronic applications.

CONCLUSION

We have developed a systematic route to highly luminescent $CsPbX_3$ nanocrystals by carefully investigating their surface chemistry through a combined experimental and theoretical study. Strong evidence was presented for surface halide vacancies as the predominant source of charge trapping. The number of trap states was quantified by ^1H NMR spectroscopy, and is broadly consistent with a simple trapping model. Trap depth varies with halide composition, thus explaining the relatively low PLQY of $CsPbCl_3$ along with the high PLQY of $CsPbBr_3$ and $CsPbI_3$. We utilized hard-soft acid base theory to develop a general X-type ligand passivation scheme that is grounded in established principles of coordination chemistry, and we showed that the tail group of carboxylates can be used to selectively coordinate or dissociate these ligands. We used these findings to prepare essentially trap-free $CsPbBr_3$ and $CsPbI_3$ nanocrystals, and although we were unable to produce near-unity PLQY $CsPbCl_3$, we identified several promising routes to be pursued. Our findings are able to unify a wide variety of reports on improved luminescence in $CsPbX_3$ materials, thereby establishing a general mechanism for the passivation of lead halide perovskite surfaces. This work not only informs future post-synthetic efforts, but synthetic efforts as well. By providing both a general passivation mechanism and the ligand exchange tools required for precise manipulations of the surface, this work opens the door to future surface investigations as well as rational improvements of photonic and optoelectronic applications based on lead halide perovskite materials.

Associated Content

Supporting Information

The Supporting Information contains experimental details and data for nanocrystal synthesis and isolation, transmission electron microscopy (TEM), nuclear magnetic resonance spectroscopy (NMR), and absolute quantum yield measurements, as well as a step-by-step guide to the ligand exchange method, computational details, and additional figures. The SI is available free of charge via the Internet at http://pubs.acs.org

Author Information

Corresponding Author

*paul.alivisatos@berkeley.edu

ORCID

David P. Nenon: 0000-0002-2045-5219

Kimo Pressler: 0000-0003-2788-1592

Jun Kang: 0000-0003-4788-0028

Brent A. Koscher: 0000-0001-8233-0852

Jacob H. Olshansky: 0000-0003-3658-1487

Wojciech T. Osowiecki: 0000-0002-7051-1768

Matthew A. Koc: 0000-0003-1401-8415

A. Paul Alivisatos: 0000-0001-6895-9048

Notes

The authors declare no competing financial interest.

Acknowledgements

This work was primarily supported by the U.S. Department of Energy, Office of Science, Office of Basic Energy Sciences, Materials Sciences and Engineering Division, under Contract No. DE-AC02-05-CH11231 (Physical Chemistry of Inorganic Nanostructures Program (KC3103)). The theoretical work was supported by the U.S. Department of Energy, Office of Science, Office of Basic Energy Sciences, Materials Sciences and Engineering Division, under Contract No. DE-AC02-05-CH11231 (Organic/Inorganic Nanocomposite Program (KC3104)). D.P.N. and J.H.O. acknowledge the National Science Foundation Graduate Research Fellowship under Grant DGE 1106400. Computational resources were provided by the National Energy Research Scientific Computing Center, a DOE Office of Science User Facility supported by the Office of Science of the U.S. Department of Energy under Contract No. DE-AC02-05-CH11231. XPS spectra were collected at the Molecular Foundry, supported by the Office of Science, Office of Basic Energy Sciences, of the U.S. Department of Energy under Contract No. DE-AC02-05CH11231. The authors would also like to thank Erin O'Brien, Justin Ondry, Colin Gould, Michael Boreen, and Nima Balan for insightful discussions, Dr. Hasan Celik and Dr. Nanette Jarenwattananon of the College of Chemistry NMR facility for their help with NMR experiments, as well as Tracy Mattox for help with XPS experiments.

References

1. Chen, O.; Zhao, J.; Chauhan, V. P.; Cui, J.; Wong, C.; Harris, D. K.; Wei, H.; Han, H.-S.; Fukumura, D.; Jain, R. K.; Bawendi, M. G., Compact high-quality CdSe–CdS core–shell nanocrystals with narrow emission linewidths and suppressed blinking. *Nat. Mater.* **2013,** *12*, 445.

2. Mahler, B.; Spinicelli, P.; Buil, S.; Quelin, X.; Hermier, J.-P.; Dubertret, B., Towards non-blinking colloidal quantum dots. *Nat. Mater.* **2008,** *7*, 659.

3. Koscher, B. A.; Swabeck, J. K.; Bronstein, N. D.; Alivisatos, A. P., Essentially Trap-Free CsPbBr3 Colloidal Nanocrystals by Postsynthetic Thiocyanate Surface Treatment. *J. Am. Chem. Soc.* **2017,** *139* (19), 6566-6569.

4. Medintz, I. L.; Uyeda, H. T.; Goldman, E. R.; Mattoussi, H., Quantum dot bioconjugates for imaging, labelling and sensing. *Nat. Mater.* **2005,** *4*, 435.

5. Bruchez, M.; Moronne, M.; Gin, P.; Weiss, S.; Alivisatos, A. P., Semiconductor Nanocrystals as Fluorescent Biological Labels. *Science* **1998,** *281* (5385), 2013-2016.

6. Murray, C. B.; Norris, D. J.; Bawendi, M. G., Synthesis and characterization of nearly monodisperse CdE (E = sulfur, selenium, tellurium) semiconductor nanocrystallites. *J. Am. Chem. Soc.* **1993,** *115* (19), 8706-8715.

7. Shirasaki, Y.; Supran, G. J.; Bawendi, M. G.; Bulović, V., Emergence of colloidal quantum-dot light-emitting technologies. *Nature Photonics* **2012,** *7*, 13.

8. Talapin, D. V.; Lee, J.-S.; Kovalenko, M. V.; Shevchenko, E. V., Prospects of Colloidal Nanocrystals for Electronic and Optoelectronic Applications. *Chem. Rev.* **2010,** *110* (1), 389-458.

9. Lee, J.; Sundar, V. C.; Heine, J. R.; Bawendi, M. G.; Jensen, K. F., Full Color Emission from II–VI Semiconductor Quantum Dot–Polymer Composites. *Adv. Mater.* **2000,** *12* (15), 1102-1105.

10. Protesescu, L.; Yakunin, S.; Bodnarchuk, M. I.; Krieg, F.; Caputo, R.; Hendon, C. H.; Yang, R. X.; Walsh, A.; Kovalenko, M. V., Nanocrystals of Cesium Lead Halide Perovskites (CsPbX3, X = Cl, Br, and I): Novel Optoelectronic Materials Showing Bright Emission with Wide Color Gamut. *Nano Lett.* **2015,** *15* (6), 3692-3696.

11. Nedelcu, G.; Protesescu, L.; Yakunin, S.; Bodnarchuk, M. I.; Grotevent, M. J.; Kovalenko, M. V., Fast Anion-Exchange in Highly Luminescent Nanocrystals of Cesium Lead Halide Perovskites (CsPbX3, X = Cl, Br, I). *Nano Lett.* **2015,** *15* (8), 5635-5640.

12. Akkerman, Q. A.; D'Innocenzo, V.; Accornero, S.; Scarpellini, A.; Petrozza, A.; Prato, M.; Manna, L., Tuning the Optical Properties of Cesium Lead Halide Perovskite Nanocrystals by Anion Exchange Reactions. *J. Am. Chem. Soc.* **2015,** *137* (32), 10276-10281.

13. Swarnkar, A.; Marshall, A. R.; Sanehira, E. M.; Chernomordik, B. D.; Moore, D. T.; Christians, J. A.; Chakrabarti, T.; Luther, J. M., Quantum dot–induced phase stabilization of α-$CsPbI_3$ perovskite for high-efficiency photovoltaics. *Science* **2016,** *354* (6308), 92-95.

14. Eaton, S. W.; Lai, M.; Gibson, N. A.; Wong, A. B.; Dou, L.; Ma, J.; Wang, L.-W.; Leone, S. R.; Yang, P., Lasing in robust cesium lead halide perovskite nanowires. *Proceedings of the National Academy of Sciences* **2016,** *113* (8), 1993.

15. Zhang, X.; Sun, C.; Zhang, Y.; Wu, H.; Ji, C.; Chuai, Y.; Wang, P.; Wen, S.; Zhang, C.; Yu, W. W., Bright Perovskite Nanocrystal Films for Efficient Light-Emitting Devices. *J. Phys. Chem. Lett.* **2016,** *7* (22), 4602-4610.

16. Li, X.; Wu, Y.; Zhang, S.; Cai, B.; Gu, Y.; Song, J.; Zeng, H., Quantum Dots: $CsPbX_3$ Quantum Dots for Lighting and Displays: Room-Temperature Synthesis, Photoluminescence Superiorities, Underlying Origins and White Light-Emitting Diodes. *Adv. Funct. Mater.* **2016,** *26* (15), 2584-2584.

17. Shi, Z.; Li, Y.; Zhang, Y.; Chen, Y.; Li, X.; Wu, D.; Xu, T.; Shan, C.; Du, G., High-Efficiency and Air-Stable Perovskite Quantum Dots Light-Emitting Diodes with an All-Inorganic Heterostructure. *Nano Lett.* **2017,** *17* (1), 313-321.

18. Kovalenko, M. V.; Protesescu, L.; Bodnarchuk, M. I., Properties and potential optoelectronic applications of lead halide perovskite nanocrystals. *Science* **2017,** *358* (6364), 745-750.

19. ten Brinck, S.; Infante, I., Surface Termination, Morphology, and Bright Photoluminescence of Cesium Lead Halide Perovskite Nanocrystals. *ACS Energy Lett.* **2016,** *1* (6), 1266-1272.

20. Kang, J.; Wang, L.-W., High Defect Tolerance in Lead Halide Perovskite $CsPbBr_3$. *J. Phys. Chem. Lett.* **2017,** *8* (2), 489-493.

21. Houtepen, A. J.; Hens, Z.; Owen, J. S.; Infante, I., On the Origin of Surface Traps in Colloidal II–VI Semiconductor Nanocrystals. *Chem. Mater.* **2017,** *29* (2), 752-761.

22. Boles, M. A.; Ling, D.; Hyeon, T.; Talapin, D. V., The surface science of nanocrystals. *Nat. Mater.* **2016,** *15*, 141.

23. Giansante, C.; Infante, I., Surface Traps in Colloidal Quantum Dots: A Combined Experimental and Theoretical Perspective. *J. Phys. Chem. Lett.* **2017,** *8* (20), 5209-5215.

24. Saba, M.; Aresti, M.; Quochi, F.; Marceddu, M.; Loi, M. A.; Huang, J.; Talapin, D. V.; Mura, A.; Bongiovanni, G., Light-Induced Charged and Trap States in Colloidal Nanocrystals Detected by Variable Pulse Rate Photoluminescence Spectroscopy. *ACS Nano* **2013,** *7* (1), 229-238.

25. Rabouw, F. T.; Kamp, M.; van Dijk-Moes, R. J. A.; Gamelin, D. R.; Koenderink, A. F.; Meijerink, A.; Vanmaekelbergh, D., Delayed Exciton Emission and Its Relation to Blinking in CdSe Quantum Dots. *Nano Lett.* **2015,** *15* (11), 7718-7725.

26. Bawendi, M. G.; Wilson, W. L.; Rothberg, L.; Carroll, P. J.; Jedju, T. M.; Steigerwald, M. L.; Brus, L. E., Electronic structure and photoexcited-carrier dynamics in nanometer-size CdSe clusters. *Phys. Rev. Lett.* **1990,** *65* (13), 1623-1626.

27. Voznyy, O.; Thon, S. M.; Ip, A. H.; Sargent, E. H., Dynamic Trap Formation and Elimination in Colloidal Quantum Dots. *J. Phys. Chem. Lett.* **2013,** *4* (6), 987-992.

28. Boehme, S. C.; Azpiroz, J. M.; Aulin, Y. V.; Grozema, F. C.; Vanmaekelbergh, D.; Siebbeles, L. D. A.; Infante, I.; Houtepen, A. J., Density of Trap States and Auger-mediated Electron Trapping in CdTe Quantum-Dot Solids. *Nano Lett.* **2015,** *15* (5), 3056-3066.

29. Hwang, G. W.; Kim, D.; Cordero, J. M.; Wilson, M. W. B.; Chuang, C.-H. M.; Grossman, J. C.; Bawendi, M. G., Identifying and Eliminating Emissive Sub-bandgap States in Thin Films of PbS Nanocrystals. *Adv. Mater.* **2015,** *27* (30), 4481-4486.

30. Gómez-Campos, F. M.; Califano, M., Hole Surface Trapping in CdSe Nanocrystals: Dynamics, Rate Fluctuations, and Implications for Blinking. *Nano Lett.* **2012,** *12* (9), 4508-4517.

31. Reiss, P.; Protière, M.; Li, L., Core/Shell Semiconductor Nanocrystals. *Small* **2009,** *5* (2), 154-168.

32. Gao, Y.; Peng, X., Photogenerated Excitons in Plain Core CdSe Nanocrystals with Unity Radiative Decay in Single Channel: The Effects of Surface and Ligands. *J. Am. Chem. Soc.* **2015,** *137* (12), 4230-4235.

33. Pu, C.; Peng, X., To Battle Surface Traps on CdSe/CdS Core/Shell Nanocrystals: Shell Isolation versus Surface Treatment. *J. Am. Chem. Soc.* **2016,** *138* (26), 8134-8142.

34. Ip, A. H.; Thon, S. M.; Hoogland, S.; Voznyy, O.; Zhitomirsky, D.; Debnath, R.; Levina, L.; Rollny, L. R.; Carey, G. H.; Fischer, A.; Kemp, K. W.; Kramer, I. J.; Ning, Z.; Labelle, A. J.; Chou, K. W.; Amassian, A.; Sargent, E. H., Hybrid passivated colloidal quantum dot solids. *Nature Nanotechnology* **2012,** *7*, 577.

35. Kilina, S. V.; Tamukong, P. K.; Kilin, D. S., Surface Chemistry of Semiconducting Quantum Dots: Theoretical Perspectives. *Acc. Chem. Res.* **2016,** *49* (10), 2127-2135.

36. Ding, T. X.; Olshansky, J. H.; Leone, S. R.; Alivisatos, A. P., Efficiency of Hole Transfer from Photoexcited Quantum Dots to Covalently Linked Molecular Species. *J. Am. Chem. Soc.* **2015,** *137* (5), 2021-2029.

37. Green, M. L. H., A new approach to the formal classification of covalent compounds of the elements. *J. Organomet. Chem.* **1995,** *500* (1), 127-148.

38. Knowles, K. E.; Frederick, M. T.; Tice, D. B.; Morris-Cohen, A. J.; Weiss, E. A., Colloidal Quantum Dots: Think Outside the (Particle-in-a-)Box. *J. Phys. Chem. Lett.* **2012,** *3* (1), 18-26.

39. Morris-Cohen, A. J.; Malicki, M.; Peterson, M. D.; Slavin, J. W. J.; Weiss, E. A., Chemical, Structural, and Quantitative Analysis of the Ligand Shells of Colloidal Quantum Dots. *Chem. Mater.* **2013,** *25* (8), 1155-1165.

40. De Roo, J.; Ibáñez, M.; Geiregat, P.; Nedelcu, G.; Walravens, W.; Maes, J.; Martins, J. C.; Van Driessche, I.; Kovalenko, M. V.; Hens, Z., Highly Dynamic Ligand Binding and Light Absorption Coefficient of Cesium Lead Bromide Perovskite Nanocrystals. *ACS Nano* **2016,** *10* (2), 2071-2081.

41. Ravi, V. K.; Santra, P. K.; Joshi, N.; Chugh, J.; Singh, S. K.; Rensmo, H.; Ghosh, P.; Nag, A., Origin of the Substitution Mechanism for the Binding of Organic Ligands on the Surface of $CsPbBr_3$ Perovskite Nanocubes. *J. Phys. Chem. Lett.* **2017,** *8* (20), 4988-4994.

42. Udayabhaskararao, T.; Houben, L.; Cohen, H.; Menahem, M.; Pinkas, I.; Avram, L.; Wolf, T.; Teitelboim, A.; Leskes, M.; Yaffe, O.; Oron, D.; Kazes, M., A Mechanistic Study of Phase Transformation in Perovskite Nanocrystals Driven by Ligand Passivation. *Chem. Mater.* **2018,** *30* (1), 84-93.

43. Woo, J. Y.; Kim, Y.; Bae, J.; Kim, T. G.; Kim, J. W.; Lee, D. C.; Jeong, S., Highly Stable Cesium Lead Halide Perovskite Nanocrystals through in Situ Lead Halide Inorganic Passivation. *Chem. Mater.* **2017,** *29* (17), 7088-7092.

44. Alpert, M. R.; Niezgoda, J. S.; Chen, A. Z.; Foley, B. J.; Cuthriell, S.; Yoon, L. U.; Choi, J. J., Colloidal Nanocrystals as a Platform for Rapid Screening of Charge Trap Passivating Molecules for Metal Halide Perovskite Thin Films. *Chem. Mater.* **2018,** *30* (14), 4515-4526.

45. Pan, J.; Sarmah, S. P.; Murali, B.; Dursun, I.; Peng, W.; Parida, M. R.; Liu, J.; Sinatra, L.; Alyami, N.; Zhao, C.; Alarousu, E.; Ng, T. K.; Ooi, B. S.; Bakr, O. M.; Mohammed, O. F., Air-Stable Surface-Passivated Perovskite Quantum Dots for Ultra-Robust, Single- and Two-Photon-Induced Amplified Spontaneous Emission. *J. Phys. Chem. Lett.* **2015,** *6* (24), 5027-5033.

46. Li, H.; Qian, Y.; Xing, X.; Zhu, J.; Huang, X.; Jing, Q.; Zhang, W.; Zhang, C.; Lu, Z., Enhancing Luminescence and Photostability of $CsPbBr_3$ Nanocrystals via Surface Passivation with Silver Complex. *J. Phys. Chem. C* **2018,** *122* (24), 12994-13000.

47. Han, G.; Koh, T. M.; Lim, S. S.; Goh, T. W.; Guo, X.; Leow, S. W.; Begum, R.; Sum, T. C.; Mathews, N.; Mhaisalkar, S., Facile Method to Reduce Surface Defects and Trap Densities in Perovskite Photovoltaics. *ACS Appl. Mater. Interfaces* **2017,** *9* (25), 21292-21297.

48. Gonzalez-Carrero, S.; Francés-Soriano, L.; González-Béjar, M.; Agouram, S.; Galian, R. E.; Pérez-Prieto, J., The Luminescence of $CH_3NH_3PbBr_3$ Perovskite Nanoparticles Crests the Summit and Their Photostability under Wet Conditions is Enhanced. *Small* **2016,** *12* (38), 5245-5250.

49. Wu, Y.; Wei, C.; Li, X.; Li, Y.; Qiu, S.; Shen, W.; Cai, B.; Sun, Z.; Yang, D.; Deng, Z.; Zeng, H., In Situ Passivation of $PbBr_6^{4-}$ Octahedra toward Blue Luminescent $CsPbBr_3$ Nanoplatelets with Near 100% Absolute Quantum Yield. *ACS Energy Lett.* **2018,** *3* (9), 2030-2037.

50. Bohn, B. J.; Tong, Y.; Gramlich, M.; Lai, M. L.; Döblinger, M.; Wang, K.; Hoye, R. L. Z.; Müller-Buschbaum, P.; Stranks, S. D.; Urban, A. S.; Polavarapu, L.; Feldmann, J., Boosting Tunable Blue Luminescence of Halide Perovskite Nanoplatelets through Postsynthetic Surface Trap Repair. *Nano Lett.* **2018,** *18* (8), 5231-5238.

51. Ahmed, T.; Seth, S.; Samanta, A., Boosting the Photoluminescence of $CsPbX_3$ (X = Cl, Br, I) Perovskite Nanocrystals Covering a Wide Wavelength Range by Postsynthetic Treatment with Tetrafluoroborate Salts. *Chem. Mater.* **2018,** *30* (11), 3633-3637.

52. Tan, Y.; Zou, Y.; Wu, L.; Huang, Q.; Yang, D.; Chen, M.; Ban, M.; Wu, C.; Wu, T.; Bai, S.; Song, T.; Zhang, Q.; Sun, B., Highly Luminescent and Stable Perovskite Nanocrystals with Octylphosphonic Acid as Ligand for Efficient Light Emitting Diodes. *ACS Appl. Mater. Interfaces* **2018**.

53. Noel, N. K.; Abate, A.; Stranks, S. D.; Parrott, E. S.; Burlakov, V. M.; Goriely, A.; Snaith, H. J., Enhanced Photoluminescence and Solar Cell Performance via Lewis Base Passivation of Organic–Inorganic Lead Halide Perovskites. *ACS Nano* **2014,** *8* (10), 9815-9821.

54. Pan, J.; Quan, L. N.; Zhao, Y.; Peng, W.; Murali, B.; Sarmah, S. P.; Yuan, M.; Sinatra, L.; Alyami, N. M.; Liu, J.; Yassitepe, E.; Yang, Z.; Voznyy, O.; Comin, R.; Hedhili, M. N.; Mohammed, O. F.; Lu, Z. H.; Kim, D. H.; Sargent, E. H.; Bakr, O. M., Highly Efficient Perovskite-Quantum-Dot Light-Emitting Diodes by Surface Engineering. *Adv. Mater.* **2016,** *28* (39), 8718-8725.

55. Pan, J.; Shang, Y.; Yin, J.; De Bastiani, M.; Peng, W.; Dursun, I.; Sinatra, L.; El-Zohry, A. M.; Hedhili, M. N.; Emwas, A.-H.; Mohammed, O. F.; Ning, Z.; Bakr, O. M., Bidentate Ligand-Passivated CsPbI3 Perovskite Nanocrystals for Stable Near-Unity Photoluminescence Quantum Yield and Efficient Red Light-Emitting Diodes. *J. Am. Chem. Soc.* **2018,** *140* (2), 562-565.

56. Di Stasio, F.; Christodoulou, S.; Huo, N.; Konstantatos, G., Near-Unity Photoluminescence Quantum Yield in $CsPbBr_3$ Nanocrystal Solid-State Films via Postsynthesis Treatment with Lead Bromide. *Chem. Mater.* **2017,** *29* (18), 7663-7667.

57. Bosch, M. P.; Perez, R.; Lahuerta, G.; Hernanz, D.; Camps, F.; Guerrero, A., Difluoropalmitic Acids as Potential Inhibitors of the Biosynthesis of the Sex Pheromone of the Egyptian Armyworm Spodoptera littoralis - IV. *Biorg. Med. Chem.* **1996,** *4* (3), 6.

58. Yang, Z. Y.; Burton, D. J., Nickel-catalyzed reaction of iododifluoroacetates with alkenes and zinc: a novel and practical route to α,α-difluoro-functionalized esters and α,α,Ω,Ω-tetrafluoro diesters. *The Journal of Organic Chemistry* **1992,** *57* (19), 5144-5149.

59. Bronstein, N. D.; Yao, Y.; Xu, L.; O'Brien, E.; Powers, A. S.; Ferry, V. E.; Alivisatos, A. P.; Nuzzo, R. G., Quantum Dot Luminescent Concentrator Cavity Exhibiting 30-fold Concentration. *ACS Photonics* **2015,** *2* (11), 1576-1583.

60. Kresse, G.; Furthmüller, J., Efficient iterative schemes for ab initio total-energy calculations using a plane-wave basis set. *Phys. Rev. B* **1996,** *54* (16), 11169-11186.

61. Kresse, G.; Joubert, D., From ultrasoft pseudopotentials to the projector augmented-wave method. *Phys. Rev. B* **1999,** *59* (3), 1758-1775.

62. Heyd, J.; Scuseria, G. E.; Ernzerhof, M., Hybrid functionals based on a screened Coulomb potential. *J. Chem. Phys.* **2003,** *118* (18), 8207-8215.

63. Perdew, J. P.; Burke, K.; Ernzerhof, M., Generalized Gradient Approximation Made Simple. *Phys. Rev. Lett.* **1996,** *77* (18), 3865-3868.

64. Anderson, N. C.; Hendricks, M. P.; Choi, J. J.; Owen, J. S., Ligand Exchange and the Stoichiometry of Metal Chalcogenide Nanocrystals: Spectroscopic Observation of Facile Metal-Carboxylate Displacement and Binding. *J. Am. Chem. Soc.* **2013,** *135* (49), 18536-18548.

65. Busby, E.; Anderson, N. C.; Owen, J. S.; Sfeir, M. Y., Effect of Surface Stoichiometry on Blinking and Hole Trapping Dynamics in CdSe Nanocrystals. *J. Phys. Chem. C* **2015,** *119* (49), 27797-27803.

66. Huang, X.; Paudel, T. R.; Dowben, P. A.; Dong, S.; Tsymbal, E. Y., Electronic structure and stability of the $CH_3NH_3PbBr_3$ (001) surface. *Phys. Rev. B* **2016,** *94* (19), 195309.

67. Ohmann, R.; Ono, L. K.; Kim, H.-S.; Lin, H.; Lee, M. V.; Li, Y.; Park, N.-G.; Qi, Y., Real-Space Imaging of the Atomic Structure of Organic–Inorganic Perovskite. *J. Am. Chem. Soc.* **2015,** *137* (51), 16049-16054.

68. Buin, A.; Pietsch, P.; Xu, J.; Voznyy, O.; Ip, A. H.; Comin, R.; Sargent, E. H., Materials Processing Routes to Trap-Free Halide Perovskites. *Nano Lett.* **2014,** *14* (11), 6281-6286.

69. Uratani, H.; Yamashita, K., Charge Carrier Trapping at Surface Defects of Perovskite Solar Cell Absorbers: A First-Principles Study. *J. Phys. Chem. Lett.* **2017,** *8* (4), 742-746.

70. Philippe, B.; Park, B.-W.; Lindblad, R.; Oscarsson, J.; Ahmadi, S.; Johansson, E. M. J.; Rensmo, H., Chemical and Electronic Structure Characterization of Lead Halide Perovskites and Stability Behavior under Different Exposures—A Photoelectron Spectroscopy Investigation. *Chem. Mater.* **2015,** *27* (5), 1720-1731.

71. Dang, Z.; Shamsi, J.; Akkerman, Q. A.; Imran, M.; Bertoni, G.; Brescia, R.; Manna, L., Low-Temperature Electron Beam-Induced Transformations of Cesium Lead Halide Perovskite Nanocrystals. *ACS Omega* **2017,** *2* (9), 5660-5665.

72. Turo, M. J.; Macdonald, J. E., Crystal-Bound vs Surface-Bound Thiols on Nanocrystals. *ACS Nano* **2014,** *8* (10), 10205-10213.

73. Turo, M. J.; Shen, X.; Brandon, N. K.; Castillo, S.; Fall, A. M.; Pantelides, S. T.; Macdonald, J. E., Dual-mode crystal-bound and X-type passivation of quantum dots. *Chem. Commun.* **2016,** *52* (82), 12214-12217.

74. Diroll, B. T.; Nedelcu, G.; Kovalenko, M. V.; Schaller, R. D., High-Temperature Photoluminescence of $CsPbX_3$ (X = Cl, Br, I) Nanocrystals. *Adv. Funct. Mater.* **2017,** *27* (21), 1606750.

75. Sebastian, M.; Peters, J. A.; Stoumpos, C. C.; Im, J.; Kostina, S. S.; Liu, Z.; Kanatzidis, M. G.; Freeman, A. J.; Wessels, B. W., Excitonic emissions and above-band-gap luminescence in the single-crystal perovskite semiconductors $CsPbBr_3$ and $CsPbCl_3$. *Phys. Rev. B* **2015,** *92* (23), 235210.

76. Shi, H.; Du, M.-H., Shallow halogen vacancies in halide optoelectronic materials. *Phys. Rev. B* **2014,** *90* (17), 174103.

77. Mizusaki, J.; Arai, K.; Fueki, K., Ionic conduction of the perovskite-type halides. *Solid State Ionics* **1983,** *11* (3), 203-211.

78. Eames, C.; Frost, J. M.; Barnes, P. R. F.; O'Regan, B. C.; Walsh, A.; Islam, M. S., Ionic transport in hybrid lead iodide perovskite solar cells. *Nature Comm.* **2015,** *6*, 7497.

79. Moreels, I.; Fritzinger, B.; Martins, J. C.; Hens, Z., Surface Chemistry of Colloidal PbSe Nanocrystals. *J. Am. Chem. Soc.* **2008,** *130* (45), 15081-15086.

80. Kim, D.; Kim, D.-H.; Lee, J.-H.; Grossman, J. C., Impact of Stoichiometry on the Electronic Structure of PbS Quantum Dots. *Phys. Rev. Lett.* **2013,** *110* (19), 196802.

81. Rogach, A. L.; Franzl, T.; Klar, T. A.; Feldmann, J.; Gaponik, N.; Lesnyak, V.; Shavel, A.; Eychmüller, A.; Rakovich, Y. P.; Donegan, J. F., Aqueous Synthesis of Thiol-Capped CdTe Nanocrystals: State-of-the-Art. *J. Phys. Chem. C* **2007,** *111* (40), 14628-14637.

82. Jones, J. W.; Gibson, H. W., Ion Pairing and Host−Guest Complexation in Low Dielectric Constant Solvents. *J. Am. Chem. Soc.* **2003,** *125* (23), 7001-7004.

83. Karmakar, A.; Askar, A. M.; Bernard, G. M.; Terskikh, V. V.; Ha, M.; Patel, S.; Shankar, K.; Michaelis, V. K., Mechanochemical Synthesis of Methylammonium Lead Mixed–Halide Perovskites: Unraveling the Solid-Solution Behavior Using Solid-State NMR. *Chem. Mater.* **2018,** *30* (7), 2309-2321.

84. Kleckner, I. R.; Foster, M. P., An introduction to NMR-based approaches for measuring protein dynamics. *Biochim. Biophys. Acta* **2011,** *1814* (8), 942-968.

85. Du, M.-H., Density Functional Calculations of Native Defects in $CH_3NH_3PbI_3$: Effects of Spin–Orbit Coupling and Self-Interaction Error. *J. Phys. Chem. Lett.* **2015,** *6* (8), 1461-1466.

86. Meggiolaro, D.; Motti, S. G.; Mosconi, E.; Barker, A. J.; Ball, J.; Andrea Riccardo Perini, C.; Deschler, F.; Petrozza, A.; De Angelis, F., Iodine chemistry determines the defect tolerance of lead-halide perovskites. *Energy & Environmental Science* **2018,** *11* (3), 702-713.

87. Azpiroz, J. M.; Ugalde, J. M.; Infante, I., Benchmark Assessment of Density Functional Methods on Group II–VI MX (M = Zn, Cd; X = S, Se, Te) Quantum Dots. *Journal of Chemical Theory and Computation* **2014,** *10* (1), 76-89.

88. Olshansky, J. H.; Ding, T. X.; Lee, Y. V.; Leone, S. R.; Alivisatos, A. P., Hole Transfer from Photoexcited Quantum Dots: The Relationship between Driving Force and Rate. *J. Am. Chem. Soc.* **2015,** *137* (49), 15567-15575.

89. Milstein, T. J.; Kroupa, D. M.; Gamelin, D. R., Picosecond Quantum Cutting Generates Photoluminescence Quantum Yields Over 100% in Ytterbium-Doped CsPbCl3 Nanocrystals. *Nano Lett.* **2018,** *18* (6), 3792-3799.

90. Yettapu, G. R.; Talukdar, D.; Sarkar, S.; Swarnkar, A.; Nag, A.; Ghosh, P.; Mandal, P., Terahertz Conductivity within Colloidal CsPbBr3 Perovskite Nanocrystals: Remarkably High Carrier Mobilities and Large Diffusion Lengths. *Nano Lett.* **2016,** *16* (8), 4838-4848.

91. Wu, K.; Liang, G.; Shang, Q.; Ren, Y.; Kong, D.; Lian, T., Ultrafast Interfacial Electron and Hole Transfer from $CsPbBr_3$ Perovskite Quantum Dots. *J. Am. Chem. Soc.* **2015,** *137* (40), 12792-12795.

92. Liu, F.; Zhang, Y.; Ding, C.; Kobayashi, S.; Izuishi, T.; Nakazawa, N.; Toyoda, T.; Ohta, T.; Hayase, S.; Minemoto, T.; Yoshino, K.; Dai, S.; Shen, Q., Highly Luminescent Phase-Stable $CsPbI_3$ Perovskite Quantum Dots Achieving Near 100% Absolute Photoluminescence Quantum Yield. *ACS Nano* **2017,** *11* (10), 10373-10383.

93. He, J.; Vasenko, A. S.; Long, R.; Prezhdo, O. V., Halide Composition Controls Electron–Hole Recombination in Cesium–Lead Halide Perovskite Quantum Dots: A Time Domain Ab Initio Study. *J. Phys. Chem. Lett.* **2018,** *9* (8), 1872-1879.

94. Owen, J., The coordination chemistry of nanocrystal surfaces. *Science* **2015,** *347* (6222), 615-616.

95. Yin, Y.; Alivisatos, A. P., Colloidal nanocrystal synthesis and the organic–inorganic interface. *Nature* **2004,** *437*, 664.

96. Hens, Z.; Martins, J. C., A Solution NMR Toolbox for Characterizing the Surface Chemistry of Colloidal Nanocrystals. *Chem. Mater.* **2013,** *25* (8), 1211-1221.

97. Panina, N. S.; Belyaev, A. N.; Simanova, S. A., Carboxylic Acids and Their Anions. Acid and Ligand Properties. *Russ. J. Gen. Chem.* **2002,** *72* (1), 91-94.

98. Siggel, M. R. F.; Streitwieser, A.; Thomas, T. D., The role of resonance and inductive effects in the acidity of carboxylic acids. *J. Am. Chem. Soc.* **1988,** *110* (24), 8022-8028.

99. Fritzinger, B.; Moreels, I.; Lommens, P.; Koole, R.; Hens, Z.; Martins, J. C., In Situ Observation of Rapid Ligand Exchange in Colloidal Nanocrystal Suspensions Using Transfer NOE Nuclear Magnetic Resonance Spectroscopy. *J. Am. Chem. Soc.* **2009,** *131* (8), 3024-3032.

100. Clore, G. M.; Gronenborn, A. M., Theory and applications of the transferred nuclear overhauser effect to the study of the conformations of small ligands bound to proteins. *Journal of Magnetic Resonance* **1982,** *48* (3), 402-417.

101. Woo, J. Y.; Lee, S.; Lee, S.; Kim, W. D.; Lee, K.; Kim, K.; An, H. J.; Lee, D. C.; Jeong, S., Air-Stable PbSe Nanocrystals Passivated by Phosphonic Acids. *J. Am. Chem. Soc.* **2016,** *138* (3), 876-883.

102. Whitham, P. J.; Marchioro, A.; Knowles, K. E.; Kilburn, T. B.; Reid, P. J.; Gamelin, D. R., Single-Particle Photoluminescence Spectra, Blinking, and Delayed Luminescence of Colloidal CuInS2 Nanocrystals. *J. Phys. Chem. C* **2016,** *120* (30), 17136-17142.

103. Bae, W. K.; Padilha, L. A.; Park, Y.-S.; McDaniel, H.; Robel, I.; Pietryga, J. M.; Klimov, V. I., Controlled Alloying of the Core–Shell Interface in CdSe/CdS Quantum Dots for Suppression of Auger Recombination. *ACS Nano* **2013,** *7* (4), 3411-3419.

104. Fischer, S.; Bronstein, N. D.; Swabeck, J. K.; Chan, E. M.; Alivisatos, A. P., Precise Tuning of Surface Quenching for Luminescence Enhancement in Core–Shell Lanthanide-Doped Nanocrystals. *Nano Lett.* **2016,** *16* (11), 7241-7247.

105. Imran, M.; Caligiuri, V.; Wang, M.; Goldoni, L.; Prato, M.; Krahne, R.; De Trizio, L.; Manna, L., Benzoyl Halides as Alternative Precursors for the Colloidal Synthesis of Lead-Based Halide Perovskite Nanocrystals. *J. Am. Chem. Soc.* **2018,** *140* (7), 2656-2664.

Table of Contents Graphic: